Journal of Nuclear Materials 498 (2018) 149–158

Contents lists available at ScienceDirect

Journal of Nuclear Materials

journal homepage: www.elsevier.com/locate/jnucmat

A novel in-situ, lift-out, three-point bend technique to quantify the mechanical properties of an ex-service neutron irradiated inconel X-750 component

C. Howard [a, *], C.D. Judge [b], D. Poff [b], S. Parker [a], M. Griffiths [c], P. Hosemann [a]

[a] University of California Berkeley Department of Nuclear Engineering, Etcheverry Hall, MC 1730, 2521 Hearst Ave., Berkeley, CA 94709, USA
[b] Canadian Nuclear Laboratories, Radiation Damage and Deformation Branch, Chalk River, Ontario K0J 1J0, Canada
[c] Department of Mechanical and Materials Engineering, Queen's University, Kingston, Ontario K7L 3N6, Canada

ARTICLE INFO

Article history:
Received 26 June 2017
Received in revised form
21 September 2017
Accepted 1 October 2017
Available online 4 October 2017

Keywords:
Small scale mechanical testing (SSMT)
Neutron irradiation
High dose
Nickel superalloys
Mechanical properties

ABSTRACT

A first of its kind small scale mechanical testing technique involving micro-three-point bending was invented, developed, and implemented on reactor irradiated, active Inconel X-750 components removed from service after approximately 53 and 67 dpa. These tests were performed at ambient room temperature in-situ using a scanning electron microscope in order to obtain live recordings of sample deformation and loading curves. Sample and testing apparatus preparation required novel lift-out and fabrication processes. Materials from two irradiation temperature regimes, low temperature (120-280 °C) and high temperature (300 ± 15 °C) were examined. Manufacturing and finishing (grinding) of this component create differences between its edge and center, so micro-specimens from both areas were extracted in order to study these differences. According to three-point beam bending theory, a 0.2% offset yield stress parameter is introduced and calculated for all specimens. Differences in mechanical properties due to irradiation temperature and dose effects were observed. Material irradiated at the higher temperature exhibited yield strength increases of ~540 MPa after 53 dpa and ~1000 MPa after 67 dpa. There was little difference (≤310 MPa) in yield strength between materials irradiated at the lower temperature at 53 dpa and 67 dpa compared with non-irradiated material. Differences in yield strengths between the edge and center of the component are retained after irradiation. The difference in yield strengths for the edge and center regions was ~740 MPa for non-irradiated material. After irradiation to a dose of 67 dpa these differences were ~570 MPa for the lower irradiation temperature and ~710 MPa for higher irradiation temperature. There were no indications of grain boundary failures via cracking except for material irradiated to 67 dpa at low temperature.

1. Introduction

Face-centered cubic (fcc), age-hardenable, nickel-based superalloys, including Inconel X-750, provide high mechanical strength and ductility [1,2], good creep properties [3], and excellent corrosion resistance at elevated temperatures [1,2]. This combination of superior properties has made them suitable for use in nuclear reactors, specifically as fasteners (bolts) [4], centering pins [5], jet pump restraints [6], tie-rods and cladding for absorber rods in light water reactors (LWRs) [7,8] as well as cable sheathing and core wires in flux detector assemblies, fuel channel garter springs, and tensioning springs in CANDU reactors [2].

Despite the positive attributes of these alloys and their common use in nuclear systems, nickel has a high cross-section for absorbing thermal neutrons and producing (n,α), (n,p) and (n,γ) reactions, and therefore generates many displaced atoms as well as H and He gas during neutron irradiation. As a result, nickel based alloys are susceptible to He and H induced degradation phenomena. In pressurized water reactors (PWRs) and boiling water reactors (BWRs), nickel alloy components are used in fuel assemblies that are limited to less than six years of in-core service [9], or they exist as peripheral components operating for the lifetime of the reactor. In CANDU reactors, nickel alloys are used as specialized components, primarily springs, both within the core and at the periphery

* Corresponding author. 3117 Etcheverry Hall, Berkeley, CA 94720-1730, USA.
E-mail address: cam7745@berkeley.edu (C. Howard).

https://doi.org/10.1016/j.jnucmat.2017.10.002
0022-3115/

of the core. Unlike traditional LWRs, CANDU reactors have a high thermal neutron flux in the reflector and core regions, leading to significant impact on the nickel alloys deployed in those areas [2].

The long-term thermal neutron irradiation effects on high nickel containing components in both the core and periphery regions of CANDU reactors [2] is more pronounced compared to other alloys with low nickel content such as ferritic and austenitic steels. Variations in temperature, neutron spectrum, and neutron flux for different components at different locations cause large variations in component performance. Although nickel alloys in PWRs and BWRs are not subjected to the same extremes of thermal neutron exposure as seen in CANDU reactors, operation of peripheral components, such as core shroud tie-rods in BWRs, for extended periods could be impacted by accelerated damage and gas production induced by the creation of ^{59}Ni after long periods of reactor operation [2]. Nickel alloys are also used in various specialized applications involving exposure to both thermal and fast neutrons to the extent that large amounts of H and He are generated [10,11].

As a result of the concerns regarding the performance of nickel alloys in service, Inconel 718 [12,13] and Inconel 600 [14] have been studied after ion irradiation. Such studies provide information on radiation effects such as point defect clustering (dislocation loops and cavities) and can also be used to understand the disordering and dissolution of the γ' and γ'' strengthening phases. Ion irradiation was never a useful tool to study the effects of irradiation on mechanical properties because of the small volumes of irradiated material involved. With the advent of nano-scale testing capabilities this limitation no longer applies. Ion irradiation still has limitations for simulating neutron radiation effects primarily because of the higher damage rates and the difficulty in achieving the correct simultaneous gas and dpa production rates. Although ion irradiation is useful one is still better off using material that has been irradiated with neutrons, either in a materials test reactor or ideally from a power reactor component of interest. Small scale mechanical testing (SSMT) is particularly suited to the study of neutron irradiated Ni alloys because the radiation fields from neutron activation products are very high.

The effects of neutron exposure on neutron irradiated materials cannot easily be assessed by conventional means involving mechanical testing of large standardized test specimens because of the time and effort to irradiate and then test specimens using materials test reactors. Irradiated material harvested from power reactor components is particularly amenable to small scale testing. Ex-service Inconel X-750 samples that have been exposed to particular doses and temperatures relevant to particular component operating conditions have been harvested from components removed from a CANDU core [15]. This study addresses the effects of irradiation on Inconel X-750 components that had been operating in core for more than ten years, removed at two distinct times at two temperature regimes, one between 120 and 280 °C and one 300 ± 15 °C, to high doses of 53 ± 2 dpa and 67 dpa respectively [2]. Due to the fact that material was not irradiated as part of a controlled experiment, there is some uncertainty on the operating conditions. Although the calculated damage dose and gas production (H and He) can be verified by dosimetry and gas measurements, temperature has to be estimated from finite element codes and the bounding temperatures of neighboring components. The temperature for the small volume of material that is ultimately sampled is also difficult to define because of temperature gradients in the components [2,15–18].

Bulk component failure strengths for these components of complex geometry and non-conventional sizes are difficult to measure. It is not possible to perform conventional mechanical tests because of the complex geometry of the components which are only 0.7–0.8 mm thick. Therefore, a non-conventional, non-standardized, first-of-its-kind "crush test" was developed in the hot cells at Canadian Nuclear Laboratories to estimate the load-bearing capabilities of the components at high dose. Also, the crush tests need large sections of springs and there is only sufficient material available to perform one or two tests for each component from each irradiation temperature and dose. Due to the high activity levels of these core components, all tests must be performed inside of hot cell facilities.

SSMT can provide multiple samples from small volumes. In this case many samples can be taken from small volumes of the component (~1 mm^3). This drastically reduces the sample volume of each specimen (in this case to ~500 μm^3) allowing the work to be performed out of the hot cell and instead inside the chamber of the Scanning Electron Microscope (SEM). In-situ testing also allows for real time observations of deformation mechanisms. A plethora of specimens can be manufactured from each extracted component and through systematic studies which take into account their microstructures, enhanced statistics can be obtained from multiple tests on the same component. Also, common metallurgical stress parameters such as yield strength can be obtained via direct observation and straightforward calculations from sample measurements in SSMTs due to their simpler stress states from which formulations have been analytically derived.

During crush testing the fracture of the components was entirely intergranular [15,16]. Transmission electron microscopy (TEM) investigations have confirmed the presence of helium bubbles in the matrix and aligned along grain boundaries and matrix-precipitate interfaces [15–18]. There were significant differences in the bubble microstructures between Inconel X-750 materials irradiated at the two nominal temperatures, with bubbles being larger and less dense at the higher temperature. The helium bubble microstructure varied within a given specimen, with larger bubble sizes and higher densities on grain boundaries and matrix-precipitate interfaces, thus supporting a He-bubble mechanism for crack propagation along grain boundaries [15,17,18].

In this study, a novel technique to perform in-situ, lift-out, three-point bend testing at room temperature in high vacuum inside of a scanning electron microscope (SEM) on both low and high temperature specimens from the edge and center of Inconel X-750 springs after doses of 53 dpa and 67 dpa has been developed and performed. This new small scale mechanical testing (SSMT) procedure quantifies changes in mechanical properties of the springs in terms of 0.2% offset yield strength as well as observes post-yield deformation behavior and helps to determine if previously observed preferential alignment of cavities and helium bubbles along grain boundaries plays a role in failure mechanisms.

2. Experimental method

2.1. As manufactured inconel X-750

Flat spacer components wrap tightly around CANDU pressure tubes to maintain an insulating gap between the hot fuel channels and cold calandria. They are manufactured from Inconel X-750, a precipitation hardened variant of Alloy-600, by a *No. 1 Temper* wire heat treatment [19], a solution heat treatment followed by a precipitation hardening step. The material is deformed prior to the final heat treatment mostly near the outer surface by coiling and surface grinding operations. The nominal chemical composition and heat treatments are shown in Table 1 [19].

The processing of Inconel X-750 leads to rich microstructure. The matrix is a *fcc* material with many deformation twins and blocky micron-sized fcc (Ti,Nb)C inclusions forming stringers in the extrusion direction. Smaller $M_{23}C_6$ (90 wt.% Cr) precipitates < 1 μm are found on the grain boundaries as well as in grain interiors. In

Table 1
Chemical composition in wt. % and heat treatments for Inconel X-750 components [19].

Element	Al	C	Co	Cr	Cu	Fe	Mn	Ni	S	Si	Ti	Nb + Ta
Concentration	0.4–1	0.08	1	14–17	0.5	5–9	1	70	0.01	0.5	2.25–2.75	0.7–1.2
Solution Treatment							1093-1204 °C					
Precipitation Hardening							732 ± 14 °C for 16.5 h, air cool					

addition, 15 nm sized ordered fcc γ′ Ni_3Al precipitates are non-uniformly distributed throughout the material. The lattice parameter difference between matrix and γ′ is 0.5%. An η-phased Ni_3Ti precipitate can be seen on grain boundaries, especially near the outer surface [20].

While the basic microstructure has been the subject of a number of prior investigations, basic grain structure EBSD analysis was performed here in our study as well. Electron Backscattered Diffraction (EBSD) scans were performed using a Zeiss Ultra Plus SEM with 15 keV e^- and a 300 nm step size to characterize the initial microstructure of the Inconel X-750 springs via three 250 μm × 250 μm area squares: one bordering the inner edge of the spring, one in the center of the spring, and one bordering the outer edge of the spring depicted in Fig. 1. Average grain sizes for each square were calculated independently via two methods: the Planimetric method calculating the number of grains per unit area, and the average grain intercept method using both horizontal and vertical lines, in order to differentiate average grain size in the radial and tangential directions. The overall average grain size for the entire spring via the Planimetric area method was found to be $d = 8.5 \pm 2.9\ \mu m$. Grains were found to be elongated by 1.3 ± 0.7 μm in the tangential direction and 2 μm smaller on average in the edge areas compared to the center region. Electron images, EBSD grain orientation maps, and average grain size in the radial and tangential directions can be seen in Fig. 1 for all three regions.

2.2. In-service damage and hydrogen and helium production

The primary radiation damage in Inconel X-750 components in nuclear reactors is in the form of atomic displacements from direct collisions with high energy neutrons (E > 0.1 MeV) that produce about 1 dpa for every year of service. This equates to approximately 25 dpa of fast neutron damage by the end of a component's design life. In addition to this baseline damage, nickel components encounter supplemental damage from thermal neutron absorption and subsequent transmutation reactions which more than double total atomic displacement damage. This additional displacement damage mostly occurs because of the displacement cascade caused by the recoil of the atom emitting either a gamma photon, proton or helium nucleus (alpha particle). The emitted particles themselves create atomic displacements but these displacements are insignificant compared to the displacements created in the recoil cascades. The emitted particles are much more important when they come to rest as hydrogen and helium gas atoms. The helium is insoluble and readily trapped by vacancies and vacancy clusters (cavities). The fate of hydrogen is more ambiguous. Hydrogen has low solubility in austenitic materials and is highly mobile at reactor operating temperatures and thus escapes readily. Some hydrogen may become trapped, however, but any effect on the properties of the component is unknown. Helium, on the other hand, is very effective at stabilizing vacancy clusters as cavities on grain boundaries.

The nuclear reactions giving rise to the enhanced atomic displacement rates and gas atom production in Inconel X-750 are described here. Nickel in its most abundant form (68.077%) exists as ^{58}Ni and undergoes the following transmutation:

$$^{58}Ni + n \rightarrow {}^{59}Ni + \gamma \quad (1)$$

The ^{59}Ni then emits hydrogen and helium by the following two reactions:

$$^{59}Ni + n \rightarrow {}^{56}Fe + {}^{4}He \quad (2)$$

$$^{59}Ni + n \rightarrow {}^{59}Co + {}^{1}H \quad (3)$$

Further displacement damage also occurs by a third reaction

$$^{59}Ni + n \rightarrow {}^{60}Ni + \gamma \quad (4)$$

The most significant contribution to total displacement damage, hydrogen, and helium production occurs via reaction (2). Over their lifetime of operation, Inconel X-750 components in the CANDU reactor core produce >20000 appm helium and >5000 appm hydrogen. The lifetime displacement damage for Inconel X-750 components in CANDU reactors is expected to be > 80 dpa [2].

2.3. CNL component tests: crush testing and microhardness testing

Bulk crush component tests and micro hardness testing was performed on ex-service material at Canadian Nuclear Laboratories (CNL). The bulk crush test apparatus, a crushed component, and mechanical data for components after 53 dpa and 67 dpa can be seen in Fig. 2 a-c. Hardness measurements from the same specimens seen in Fig. 2d show that components irradiated at the lower temperature are softer (~365 VHN) compared to the materials irradiated at higher temperatures (~420-450 VHN) at the highest dose. In addition, cracks have formed adjacent to indents performed on the higher dose material, indicating that plastic flow is accommodated by a combination of both slip and micro-cracking.

Component crush testing seen in Fig. 2c shows that springs irradiated at the higher temperature exhibit lower strength and ductility compared to springs irradiated at the lower temperature. Extended service results in reduced strength and ductility. In the case of specimens irradiated at an average of 180 °C, ductility decreases by a factor of two after 53 dpa and nearly vanishes by 67 dpa. However, specimens irradiated at an average of 300 °C have completely lost ductility by 53 dpa. More dose results in further loss of strength.

Let it be noted that the hardness data and component crush test data follow opposite trends. Specimens irradiated at higher temperatures have higher hardness values but lower crush test failure loads. This suggests that hardening mechanisms with the bulk matrix material of the components are much different than ultimate failure mechanisms. The former is dictated by the production and distribution of point defects, dislocations, and dislocation loops, whereas the latter is dictated by grain boundary strength.

2.4. Micro- three-point bend specimen sample preparation

This study focuses on Inconel X-750 flat spring material under two irradiation conditions: approximately 53 dpa and 18000 appm helium (taken from the center of the spring labelled “C” in Fig. 1) and approximately 67 dpa and 20000 appm (taken from both the center, “C”, and edge regions of the spring) and non-irradiated material (taken from both the center and edge regions of the spring). Center

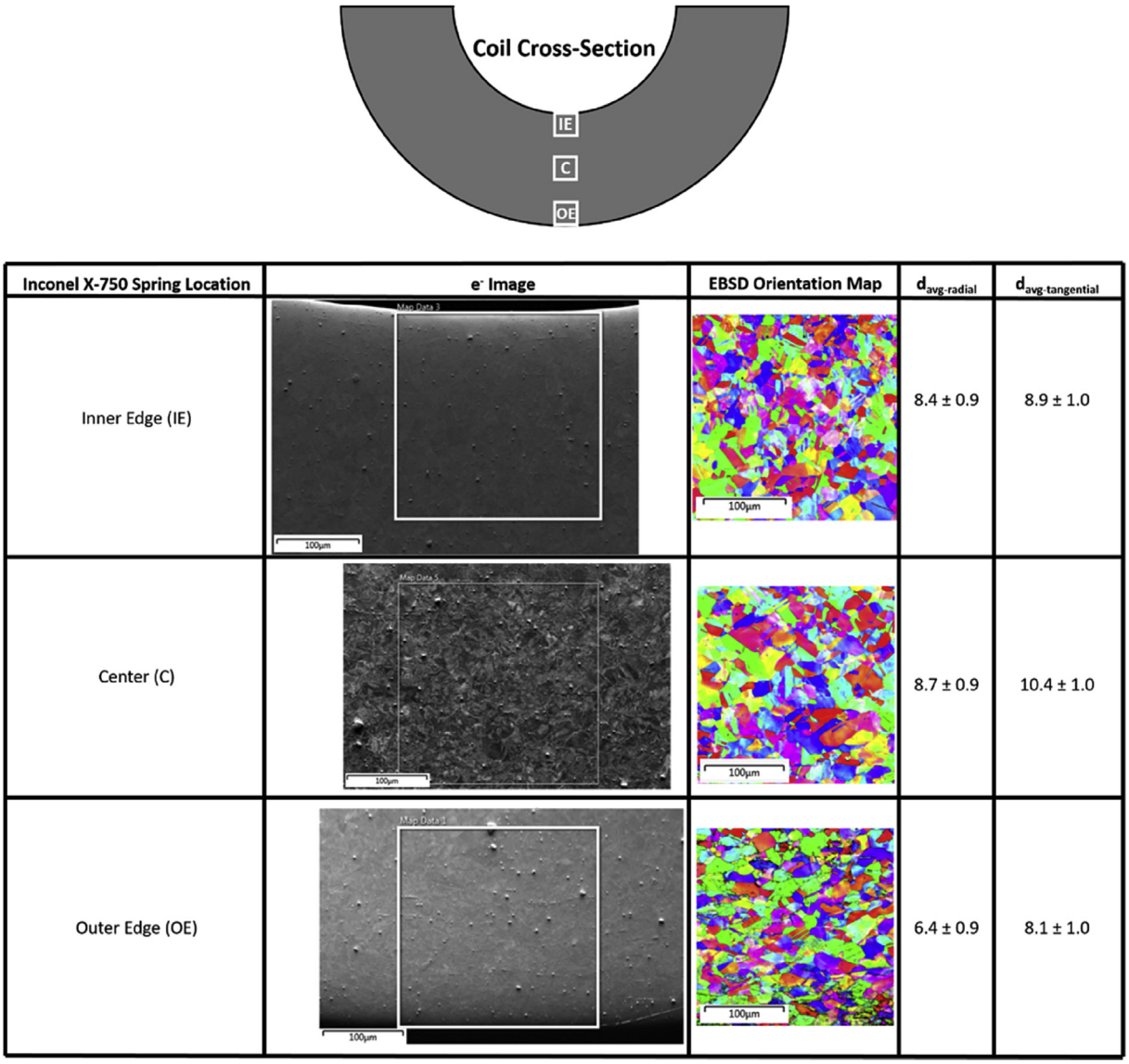

Fig. 1. Schematic of the sectioned and polished Inconel X-750 coil and Electron Backscattered Diffraction (EBSD) areas. These areas are 250 μm × 250 μm squares of the inner edge (IE), center (C), and outer edge (OE) regions of an Inconel X-750 flat spring. EBSD orientation map grain analysis produces an average overall grain size of 8.5 ± 2.9 μm and indicates grain elongation in the tangential direction.

and edge regions where materials were extracted are pictured using a representative cross-section schematic of a spring component in Fig. 1 and again using a representative irradiated cross-section electron image in Fig. 3a. For the irradiated specimens, materials that had been operating at temperatures 120-280 °C and 300 ± 15 °C [2] were investigated. A FEI Quanta 3-D Focused Ion Beam (FIB) and Oxford OmniProbe at Idaho National Laboratory (INL) were used to extract 40 μm × 20 μm x 10 μm foils of material from the center and edge regions of the irradiated springs. Pre-fabricated slots were cut into molybdenum lift-out grids using the FIB and the lifted-out foils were adhered to these sites using the platinum-based gas injection system (GIS). These large foils were then shipped to UC Berkeley for further preparation.

Three-point bend specimens were manufactured from the large foils using an in house machined 90° SEM holder inside a FEI Quanta 3D FEG with a Ga^{69+} FIB. Initially, larger milling currents (3-7 nA) were used to cut rough beams of approximate dimensions 20 μm × 7 μm x 7 μm. Resulting bar shapes cut into the large foil can be seen in Fig. 3b.

Each bar specimen similar to the two shown in Fig. 3b was subsequently lifted out using an OmniProbe 200 Nanomanipulator and mounted on a pre-fabricated bridge test site as shown in Fig. 3c. The lift-out bars were attached using the Pt GIS and final polishing occurred using smaller milling currents (100 pA-1 nA). The amount of Pt GIS deposition was kept to a minimum in an attempt to reduce its effect on the three-point bending stress state. However, this attachment is required in order to prevent the loss of samples during the mounting process and/or transfer between FIB milling and testing. This process and an example of a finished three-point bend specimen can be seen in Fig. 3. The final three-point bend specimens were approximately 15–20 μm in bending length and 3-5 μm in width and thickness.

2.5. Electron Backscattered Diffraction (EBSD) specimen pre-test analysis

Each micro-bend specimen was analyzed using EBSD on its top surface using an acceleration voltage of 30 keV, electron current of

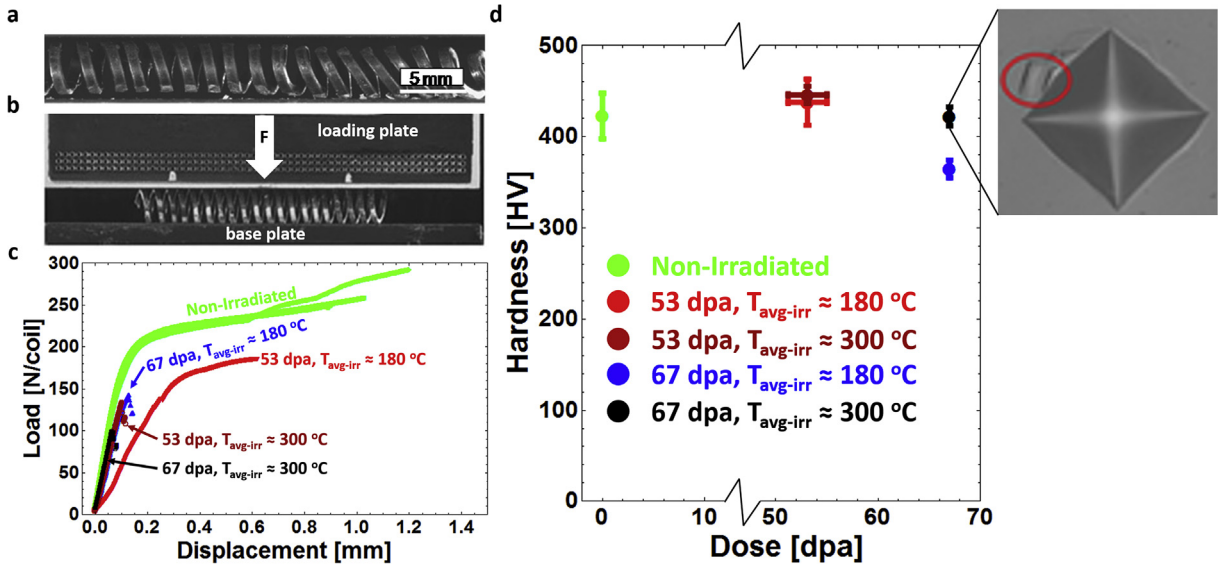

Fig. 2. Bulk crush testing of Inconel X-750 annulus spacers. (a) post-test coil, (b) close-up view of testing rig pre-test depicting the loading direction, (c) representative load-displacement curves of specimens at each irradiation condition, (d) Vickers indentation microhardness values (500 gf) of specimens at each irradiation condition with an insert depicting a representative indent where cracking occurred adjacent to the indent in the 67 dpa material irradiated at 300 °C. Cracks have developed around the surfaces of indents performed on material with a dose of 72 dpa.

48 nA, and step size ≤ 50 nm in order to map each sample's initial microstructure, identify grain boundaries, and determine grain orientations. The individual specimens were found to contain between one and five grain boundaries. Grain orientations at the bottom surface of the specimens would be more accurate, but performing EBSD on the bottom surface of the specimens is impossible due to shadowing from sample supports. However, Focused Ion Beam (FIB) ion channeling contrast images of the front and back sides of the specimens were obtained in order to ensure that grain boundaries propagated approximately straight down through the thicknesses of the specimens. Representative FIB ion channeling contrast images of the sides of polished bending specimens with grain boundaries clearly visible can be seen in Fig. 3e and f. Using these grain orientation maps, the *hkl* orientations, grain rotation, and highest Schmid factor of the preferred slip system(s) for each grain was calculated for the outward tensile stress direction at the bottom of the specimens. In addition, misorientation angles between two grains were measured. A representative depiction of the pre-test microstructural analysis can be seen in Fig. 4. Nearly all grain boundaries in the specimens that were not twin boundaries were measured to be high angle grain boundaries with misorientation angles greater than ~28°. Table 2 gives the root mean squared (RMS) absolute and normalized grain rotation within a single grain interior for specimens at each irradiation condition. Normalized average grain rotations exceed 1°/μm in edge specimens for both non-irradiated and high dose conditions. This indicates that grains at the edges of the component are more heavily deformed (by at least 0.4°/μm) due to cold-working and grinding manufacturing processes, whereas grains in the center of the component are much less deformed.

2.6. In-situ three-point bend testing

Two to five specimens made from both center and edge regions of a non-irradiated spring and 67 dpa irradiated spring, and from the center of 53 dpa springs were bent at their centers under vacuum in a FEI Quanta 3D FEG using a Hysitron PI 85 Picoindenter. The actuator was equipped with a custom made 1 μm thick and 12 μm wide diamond wedge punch. Two sets of irradiated specimens were produced and tested; the first set from material with a low irradiation temperature (180 °C) and the second from material with a high irradiation temperature (300 °C). Videos were recorded for all tests for further analysis using the Scanning Electron Microscope (SEM) on the FEI Quanta 3D FEG. All tests were performed in displacement controlled feedback loop mode at loading and unloading rates of 10 nm/s to maximum strains larger than 10% or until noticeable plastic deformation occurred. Equivalent strain rates were between 1×10^{-3} and 2×10^{-3}. In order to ensure proper sample to tip alignment the PI 85 was tilted inside the SEM chamber to 8-15° to allow simultaneous imaging of the sample and indenter with both the SEM and FIB beams. The recorded force vs. displacement curves were converted into flexural stress vs. flexural strain curves for the center point at the outer fiber of the beam using the following equations from standard three-point bending flexural theory:

$$\sigma = \frac{3FL}{2bd^2} \tag{5}$$

$$\varepsilon = \frac{6\,D\,d}{L^2} \tag{6}$$

where F is the recorded displacement in N, L the length of the specimen in mm, b the specimen width in mm, d the specimen height in mm, D the recorded displacement at the midpoint in mm, σ the stress at the midpoint in MPa, and ε the strain in the outer surface at the midpoint. The linear elastic loading portions of each curve were fit to linear regression lines of the form $\sigma = Y\,\varepsilon + A$, where σ is stress, Y is the effective specimen stiffness parameter, ε is strain, and A is an offset parameter. A 0.2% offset from this linear elastic loading regime was applied much like in ASTM tensile testing to acquire an effective specimen yield strength (σ_y). Let it be noted that due to the Pt GIS attachments, these equations serve as rough approximations of the tensile stresses at the outer fiber midpoint. Deformation of the attachments themselves as the beams are bending create complications that cannot be easily

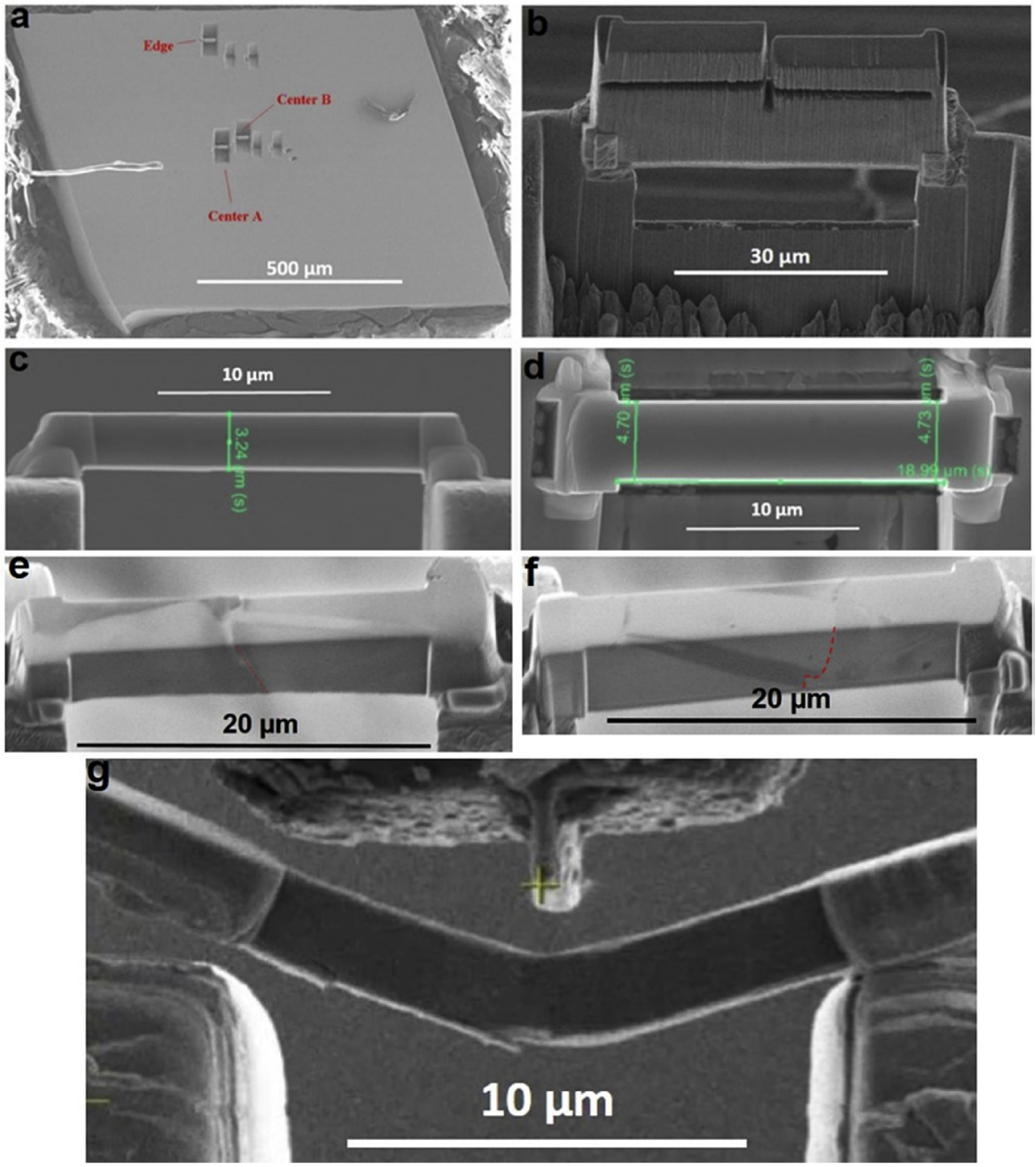

Fig. 3. (a) cross-section of an Inconel X-750 spring showing FIB milled foils of material taken from both edge and center regions (b) resulting bending beam structures cut into the large lift-out foil which has already been removed from the bulk spring (c) side view of a finished three-point bend specimen (d) top view of a completed three-point bend specimen, (e) and (f) FIB ion channeling contrast images depicting grain boundaries propagating approximately straight down through the thickness of the specimens, and (g) bending specimen becomes unconstrained similar to a standard three-point bend test during loading.

accounted for by analytical expressions. However, as seen in Fig. 3g, bending specimens do become unconstrained during testing such that they begin to parallel a standard three-point bend test.

3. Results

Representative flexural stress-strain responses of tests on specimens from each dose and temperature condition can be seen in Fig. 5. For all tests, complete fracture of the specimens did not occur. In all cases dislocation slip on parallel slip planes along the deformed specimens was observed in real time as imaged by the SEM and in post-test SEM images. A summary of average 0.2% offset yield strength values for all irradiation conditions and spring locations can be found in Table 3.

The results shown in Fig. 5 and Table 3 reveal a dramatic pre-existing, non-uniform, cold-working effect on the mechanical properties of Inconel X-750 springs. Material in the edge region of the spring was measured to be approximately 740 MPa stronger than material in the center of the spring. As the radiation dose on the component increases, this pre-existing effect remains as seen in the 67 dpa material. A difference in yield strengths between 67 dpa edge and center materials of 712 MPa occurs in the material with a higher irradiation temperature (300 ± 15 °C), and the material with a lower irradiation temperature (120-280 °C) still retains this difference as well. Edge material irradiated to 67 dpa is 566 MPa stronger compared to the center.

A matrix radiation strengthening effect with increasing dose is evident in all high temperature specimens, whereas changes in yield strengths of low temperature specimens appears either negligible or much subtler. High temperature center components irradiated to 53 dpa become strengthened by 540 MPa, and there is a further 530 MPa increase in yield between 53 dpa and 67 dpa components.

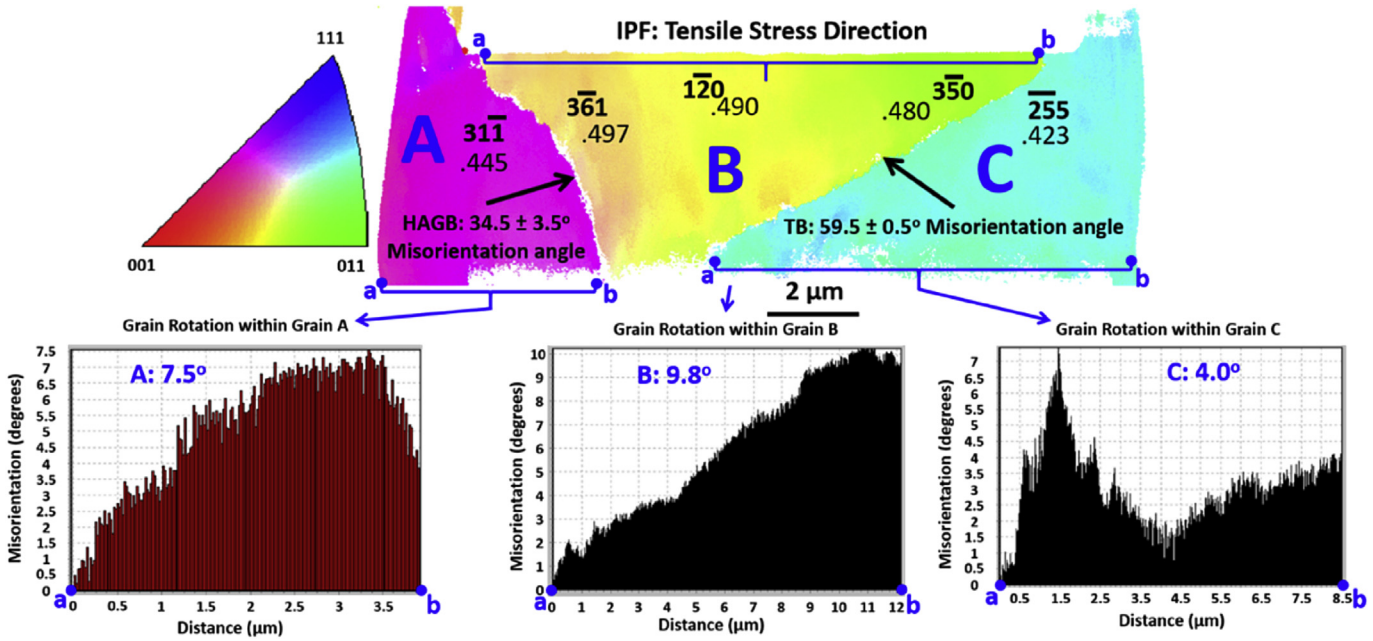

Fig. 4. Pre-test Electron Backscattered Diffraction (EBSD) on the top surface of a representative three-point bend specimen including an Inverse Pole Figure (IPF) grain orientation map in the tensile stress direction for the outer fiber of the specimen, hkl orientation of individual grains, misorientation angles across grain boundaries, grain rotation within each grain measured along a horizontal line segment left to right from point a to point b, and highest Schmid factor of the preferred slip system(s) within each grain.

Table 2
Root-mean-squared absolute and normalized grain interior misorientations of inconel X-750.

Irradiation Condition	Non-Irradiation		53 dpa T_{avg}=180 °C	53 dpa T_{avg} = 300 °C	72 dpa T_{avg} = 180 °C		72 dpa T_{avg} = 300 °C	
Spring Location	Edge	Center	Center	Center	Edge	Center	Edge	Center
θ_{rms} (degrees)	5.4° ± 4.5°	5.2° ± 2.0°	3.4° ± 1.9°	2.5° ± 1.7°	6.5° ± 3.2°	2.6° ± 1.3°	6.7° ± 2.1°	2.3 ± 0.9
θ_{rms}/L(degrees/µm)	2.4 ± 5.2	0.6 ± 0.4	0.1 ± 0.1	0.4 ± 0.3	1.7 ± 1.4	0.5 ± 0.2	0.6 ± 0.3	0.2 ± 0.1

Overall, this indicates a 1070 MPa increase between non-irradiated and highest dose center specimens. A similar effect is seen in the edge specimens; an approximate 1 GPa increase of yield strength is seen over 67 dpa. However, for low temperature material, non-irradiated, 53 dpa, and 67 dpa center specimens all have similar yield strength values. Edge region low temperature specimens also show similar yields before irradiation and after 67 dpa.

4. Discussion

Because the initiation of plastic deformation at the yield point is dislocation slip in the region of the specimens directly below the actuator at the outer fiber (highest stress point), an approximation was made that all deformation up until and including the yield point (elastic deformation and the onset of plastic deformation) occurs locally in individual grains below the loading location. Since only a limited number of grains are deformed, it is preferable to take the crystal orientation into account and compare a critical resolved shear stress (CRSS) rather than a yield stress or flexural bending stress. Based on this assumption, critical resolved shear stress (CRSS) values were calculated for the outer fibers of the specimens at the highest stress points using the highest Schmid factors of the grains beneath the wedge punch where slip planes were observed. All 12 possible *fcc* slip directions and slip planes were taken into account. It is assumed that the outer most fiber of the bend bar is in pure tension. These values are reported in the final row of Table 3, and the associated loading curves can be seen in Fig. 5c and d. It is evident that high temperature components irradiated to doses of 67 dpa necessitate higher CRSS values in order to yield. Increases of 486 MPa in edge components and 421 MPa in center components are observed. However, this approximation produces CRSS values for low temperature components that increase by ~160 MPa within the first 53 dpa and do not change with increased dose. This may suggest a saturation with respect to dose effects in low temperature components. Nonetheless, this approximation may be oversimplified, whereas a complex crystal plasticity model would be needed in order to map out the grain orientations, grain boundaries, and grain boundary planes for each specimen in order to fully characterize the result. However, such a model is not part of this study.

For all irradiated specimens, the results suggest that the material operating at a lower irradiation temperature has a lower yield stress compared to the high temperature material irradiated to the same dose. Low temperature material yields approximately 300 MPa lower than high temperature material in the same location (center or edge) irradiated to a dose of 53 dpa. For the highest dose material irradiated to 67 dpa, low temperature edge components yield ~800 MPa lower than high temperature edge components, and similarly low temperature center components are ~760 MPa weaker than high temperature center components. Conventional radiation effects in materials suggest that radiation strengthening is a function of defect cluster density [21–26], and it is well known that defect cluster density decreases as irradiation temperature increases [27–29]. The yield strength itself decreases with increasing irradiation temperature except under particular conditions for some γ′ containing superalloys, where the γ′

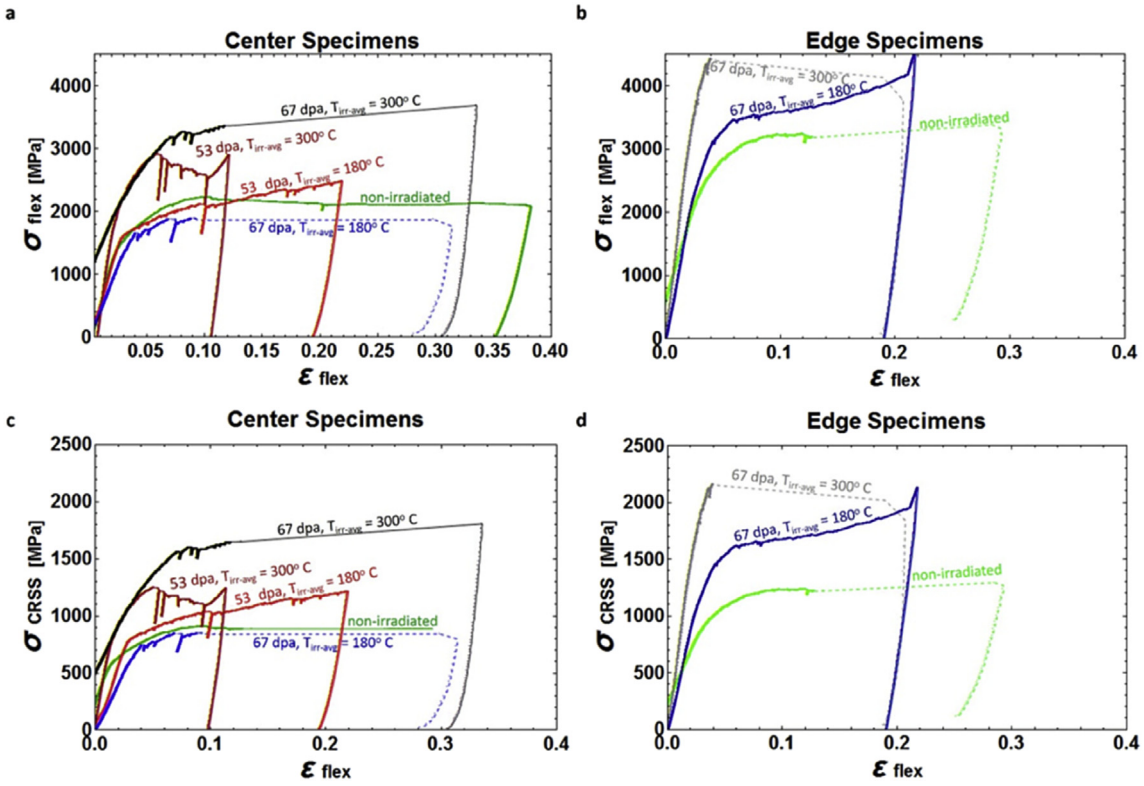

Fig. 5. Representative flexural stress-strain curves calculated for the midpoint at the outer fiber of the (a) center and (b) edge specimens according to three-point bend theory for each irradiation condition. Loading curves plotted in terms of the critical resolved shear stress (CRSS) calculated from the matrix orientation at the highest stress point can be seen for the center specimens in (c) and edge specimens in (d).

Table 3
Yield strength and critical resolved shear stress (CRSS) of inconel X-750 spring material.

Irradiation Condition	Non-Irradiation		53 dpa T_{avg}=180 °C	53 dpa T_{avg} = 300 °C	67 dpa T_{avg} = 180 °C		67 dpa T_{avg} = 300 °C	
Spring Location	Edge	Center	Center	Center	Edge	Center	Edge	Center
Number of Tests	5	4	2	4	2	2	2	2
$\sigma_{y\text{-}0.2\%\ offset}$ (MPa)	2074 ± 309	1335 ± 63	1561 ± 12	1875 ± 70	2211 ± 166	1645 ± 154	3020 ± 509	2406 ± 150
σ_{CRSS} (MPa)	935 ± 162	597 ± 28	763 ± 7	807 ± 42	988 ± 173	757 ± 77	1421 ± 323	1018 ± 95

precipitates with a sufficient size and density can suppress the decrease in yield strength with increasing temperature [30]. In 304 stainless steel, which has a similar vacancy migration energy compared to the Inconel X-750 material studied here, for irradiation doses greater than or equal to 10 dpa, the steel is softer after irradiation at ~200 °C compared with ~300 °C [31].

The yield strength for the Inconel X-750 spring material investigated here is consistent with the effects described in Ref. [31]. The high temperature material had an irradiation temperature of approximately 300 °C, whereas the low temperature material had an irradiation temperature of approximately 180 °C. According to [31], this difference in irradiation temperature would mean that one would expect the low temperature material to yield at an approximate stress of 90% of the yield of the high temperature material. Although this model has been developed for austenitic stainless steels, the Inconel X-750 low temperature material yields at 83% of the high temperature material at 53 dpa, and ~70% of the high temperature material at 67 dpa suggesting similar effects here.

This increasing strength with increasing temperature relationship is also supported by microstructural observations reported in Ref. [18]. Due to vacancy migration energies, at lower irradiation temperatures, the material is in a recombination dominated regime, whereas at higher irradiation temperatures the material is in a sink dominated regime. Thus, when interstitial clusters first form in the low temperature material, they are often annihilated through recombination, whereas in the high temperature material, they survive to form dislocation loops. In addition, the lower temperature of the material may allow for more disordering and dissolution of precipitate structures. Finally, cavity densities are much higher but individual cavity sizes are much smaller for the low temperature material, meaning they are more evenly distributed [17,18]. Overall, the matrix microstructure is much cleaner and more homogeneous in the low temperature material, leaving less obstacles to be overcome during loading deformation, less necessity for dislocation climb of network dislocations, and ultimately a softer matrix material with a lower yield strength value.

The results from the in-situ three-point bend specimens showing a higher room temperature yield stress at higher irradiation temperatures are in agreement with room temperature hardness measurements from high fluence material shown in Fig. 2d. However, the failure behavior of the specimens seen in Fig. 2c has the opposite trend with respect to temperature. This is most likely because the failure load is dependent on the grain boundary strength, which is not necessarily governed by the

same microstructural differences that are affecting the matrix yield strength.

Ultimately, the mechanisms for matrix yielding and ultimate failure of neutron irradiated Inconel X-750 spacers are different. Matrix yielding is initially governed by the spacing of ordered second phase γ' precipitates, but irradiation damage creates a different effective defect spacing which governs the new yielding behavior as this precipitation hardened phase loses its order with increasing dose [18,32–34]. It is surmised that ultimate failure is a result of intergranular fracturing. It is hypothesized that intergranular failure may be caused by helium preferentially aligning along and weakening grain boundaries is also supported by TEM investigations in Refs. [2,15–18]. The matrix strength is dominated by microstructural features other than cavities (dislocation loops and precipitates) and the radiation-induced changes in these features have a different temperature dependence [10,11,15,17,18].

Two high temperature bending specimens irradiated to a dose of 53 dpa were sharply notched in their centers at the bottom using the FIB such that the notches were located inside of single grains. These notches were confirmed to be within single grains using high resolution FIB ion channeling contrast images of the sides of the specimens. Tests of these two notched specimens did not generate cracking from the notch. Since it is known that notch tips were located inside the grain, no cracking from the notch and significant plastic deformation after yielding suggests that the matrix material has high resistance to cracking under irradiated conditions.

However, in the case of the low temperature specimens irradiated to 67 dpa, cracks developed on the bottom of both center and edge specimens. Based on the grain boundary locations indicated by EBSD scans of the top surfaces of the specimens, it is likely that the cracks follow the paths of the grain boundaries, but definite proof is difficult since EBSD after deformation is not possible due to the fact that the top sample surface, the only one which remains unblocked by sample mounts, is no longer flat. Fig. 6 shows representative center and edge specimens for low temperature material irradiated to 67 dpa with cracks that are believed to have propagated along grain boundaries and exited at the bottom of the specimens. Associated stress values for crack initiation are larger than the associated yield stresses: ~3.5 GPa for edge specimens and ~2.5 GPa for center specimens. EBSD images of side and bottom surfaces are not possible due to shadowing effects from sample holders and mounts.

To summarize initial discoveries made on the failure mechanisms of the Inconel X-750 spacers, let it be noted that there was no indication of grain boundary failure in the tests of non-irradiated specimens even when strained well beyond their yield points, but there were multiple indications of cracking along grain boundaries in the irradiated micro-scale tests seen in Fig. 6. This could be linked

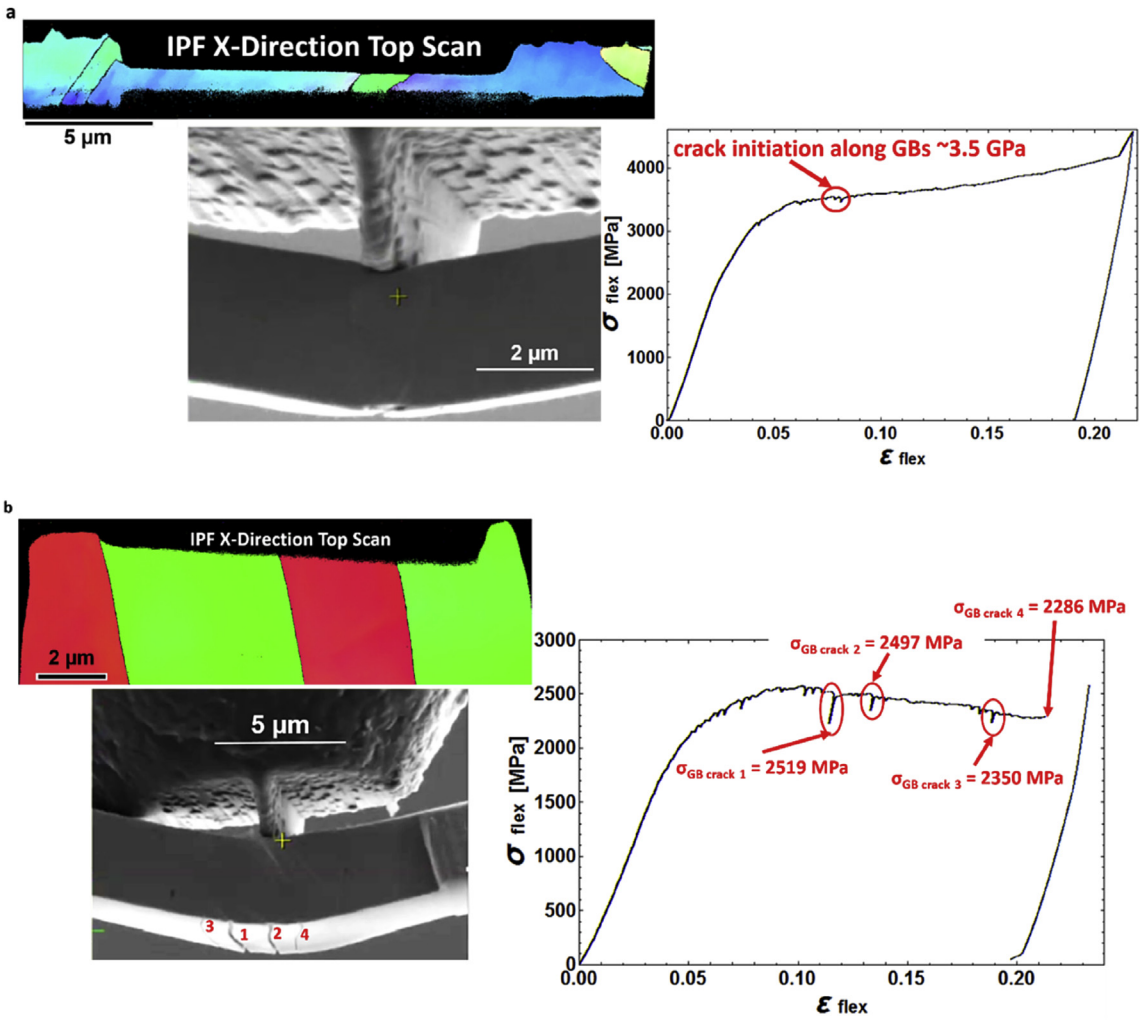

Fig. 6. Representative low temperature 67 dpa specimens with cracks along grain boundaries. (a) specimen made from spring edge with cracks along grain boundaries initiating at ~3.5 GPa (b) specimen made from spring center with cracks along grain boundaries initiating at ~2.5 GPa.

to the intergranular failure seen in macroscopic crush tests of irradiated specimens, the loading curves of which are seen in Fig. 2c, particularly in the case of low temperature specimens irradiated to 67 dpa.

5. Conclusion

A novel small scale mechanical testing (SSMT) technique involving in-situ, micro-scale, lift-out, three-point bend test experiments at room temperature in an SEM was developed and applied to assess the mechanical properties of Inconel X-750 material removed from the core of a CANDU reactor after doses of 53 dpa and 67 dpa. A systematic study was performed by extracting material from the edge and center region of the spring spacers from components that had operating temperatures of 180 °C and 300 °C on average. Quantitative mechanical properties measurements, namely 0.2% offset yield strength values, indicate obvious temperature and dose effects. The high temperature material undergoes more severe radiation strengthening, more than 1 GPa over doses up to 67 dpa, whereas strengthening of the low temperature material appears much more minimal (200-300 MPa). Pre-existing mechanical differences created by cold working spring manufacturing processes remain after extended time in the CANDU core. Yield strengths of center and edge regions of the spring differ by ~740 MPa when it is non-irradiated. This difference remains up to the highest dose components; it is larger than 700 MPa for high temperature components and ~570 MPa for low temperature components. This lift-out three-point bend testing technique did not show any indications of grain boundary failure in non-irradiated specimens, but evidence of grain boundary cracking post-yield was observed in low temperature 67 dpa specimens.

Acknowledgements

The authors of this manuscript would like to acknowledge Canadian Nuclear Laboratories for their donation of sample material and the Nuclear Science User Facility (NSUF) sample library at Idaho National Lab (INL) operated through the U.S. Department of Energy (DOE) Rapid Turnaround Post-Irradiation Experiment (RT-PIE) for instrument time, sample management and preparation. In addition, we acknowledge the support from the DOE Office of Nuclear Energy's Nuclear Energy University Program (NEUP) (DE-NE0000702). James W. Madden, microscopist at the Materials Fuels Complex (MFC) at INL, is acknowledged for his work in extracting samples and sending them to our facility at UC Berkeley. Grant Bickel and Don Metzger are acknowledged for useful discussion, Marc Paulseth for temperature estimates and R. Beier and Heygaan Rajakumar for hardness measurements. The authors would like to thank the CANDU Owners Group (COG) (JP4452) for financial support for some of this work and permission to use the data. Partial funding for this research was also provided by the Nuclear Regulatory Commission (NRC) fellowship fund. In addition, the authors would like to thank the Biomolecular Nanotechnology Center (BNC) at the University of California, Berkeley (UCB) for the use of the FEI Quanta 3D FEG.

References

[1] W.J. Mills, Mastel Bernard, Deformation and fracture characteristics for irradiated Inconel X-750, Nucl. Technol. 73.1 (1986) 102–108.
[2] M. Griffiths, The effect of irradiation on Ni-containing components in CANDU® reactor cores: a review, AECL Nucl. Rev. 2 (1) (2013).
[3] L.C. Walters, W.E. Ruther, In-reactor stress relaxation of Inconel X-750 springs, J. Nucl. Mat. 68 (1977) 324–333.
[4] J.J. Olivera, et al., Failure of Inconel X-750 bolts of internals of the CHOOZ-A nuclear power plant. CEA Centre d'Etudes Nucleaires de Fontenay-aux-Roses, 92 (France). Dept. d'Analyse de Surete, 1989.
[5] Balog, Leonard J., and David E. Boyle. Four pin mounting system for nuclear reactor control rod guide tubes. U.S. Patent No. 4,937,039. 26 Jun. 1990..
[6] Katayama, Yoshinori, et al. Jet Pump Beam and Method for Producing the Same. U.S. Patent No. 8,879,683. vol. 4 Nov. 2014..
[7] Fanning, Alan W., William G. Jameson Jr, and Victor E. Hazel. "Nuclear Fuel Assembly. U.S. Patent No. 4,314,884. vol. 9 Feb. 1982..
[8] Kim, Young Jin, et al, Fuel Rod Assembly and Method for Mitigating the Radiation-enhanced Corrosion of a Zirconium-based Component. U.S. Patent No. 8,792,607. vol. 29 Jul. 2014..
[9] Marcus Nichol, NEI Nuclear Notes Interview vol. 8, May 2012. http://neinuclearnotes.blogspot.ca/2012/05/what-happens-during-refueling-outage.html.
[10] Bulent H. Sencer, et al., Microstructural evolution of Alloy 718 at high helium and hydrogen generation rates during irradiation with 600–800 MeV protons, J. Nucl. Mater. 283 (2000) 324–328.
[11] Flavio Carsughi, et al., Investigations on Inconel 718 irradiated with 800 MeV protons, J. Nucl. Mater. 264 (1) (1999) 78–88.
[12] N. Hashimoto, et al., Microstructural analysis of ion-irradiation-induced hardening in Inconel 718, J. Nucl. Mater. 318 (2003) 300–306.
[13] J.D. Hunn, et al., Ion-irradiation-induced hardening in Inconel 718, J. Nucl. Mater. 296.1 (2001) 203–209.
[14] Ji-Jung Kai, R.D. Lee, Effects of proton irradiation on the microstructural and microchemical evolution of Inconel 600 alloy, J. Nucl. Mater. 207 (1993) 286–294.
[15] M. Griffiths, G.A. Bickel, S.A. Donohue, P. Feenstra, C.D. Judge, D. Poff, L. Walters, M.D. Wright, L.R. Greenwood, F.A. Garner, Degradation of Ni-alloy Components in a CANDU Reactor Core, 16th Int. Symposium on Environmental Degradation in Materials, 2013. Asheville, NC.
[16] C.D. Judge, M. Griffiths, L. Walters, M. Wright, G.A. Bickel, O.T. Woo, M. Stewart, S.R. Douglas, F. Garner, Embrittlement of nickel alloys in a CANDU reactor environment, in: T. Yamamoto (Ed.), Effects of Radiation on Nuclear Materials vol. 25, ASTM International, Anaheim, CA, 2012, pp. 161–175.
[17] C.D. Judge, N. Gauquelin, L. Walters, M. Wright, J.I. Cole, J. Madden, G.A. Botton, M. Griffiths, Intergranular fracture in irradiated Inconel X-750 containing very high concentrations of helium and hydrogen, J. Nucl. Mater. 457 (2015) 165–172.
[18] H.K. Zhang, Z. Yao, G. Morin, M. Griffiths, TEM characterization of in-reactor neutron irradiated CANDU spacer material Inconel X-750, J. Nucl. Mater 451 (2014) 88–96.
[19] Special Metals Corporation Publication No SMC-067, September 2004..
[20] O.T. Woo, et al., The microstructure of unirradiated and neutron irradiated Inconel X750, Microsc. Microanal. 17 (Suppl 2) (2011).
[21] T.J. Koppenaal, R.J. Arsenault Metall, Rev 16 (1971) 175.
[22] A.L. Bement Jr., W.C. Leslie (Eds.), Second International Conference on Strength of Metals and Alloys vol. II, American Society for Metals, Metals Park, OH, 1970, p. 693.
[23] U.F Kocks Mater, Sci. Eng. 27 (1977) 291.
[24] A.K. Seeger, Second UN Conference on Peaceful Uses of Atomic Energy vol. 6, United Nations, New York, 1958, p. 250.
[25] J Friedel Dislocations Pergamon, New York (1964).
[26] F. Kroupa, P.B. Hirsch Disc, Faraday Soc. 38 (1964) 49.
[27] K. Farrell, T.S. Byun, N. Hashimoto, Oak Ridge National Lab., Oak Ridge, TN Report ORNL/TM-2002/63, 2003.
[28] S.J. Zinkle, et al., in: Microstructures of Irradiated and Mechanically Deformed Metals and Alloys: Fundamental Aspects. MRS Proceedings vol. 792, Cambridge University Press, 2003.
[29] N. Hashimoto, et al., Deformation mechanisms in 316 stainless steel irradiated at 60 C and 330 C, J. Nucl. Mater. 283 (2000) 528–534.
[30] R.C. Read, The Superalloys, Fundamentals and Applications, Cambridge University Press, 2006 isbn-13 978-0-511-24546-6.
[31] G.E. Lucas, The evolution of mechanical property change in irradiated austenitic stainless steels, J. Nucl. Mater. 206-2 (1993) 287–305.
[32] L.E. Thomas, S.M. Bruemmer, Radiation-induced Microstructural Evolution and Phase Stability in Ni-base Alloy 718", Eighth International Symposium on Environmental Degradation of Materials in Nuclear Power Systems, ANS, 1997, p. 772.
[33] M.L. Hamilton, F.A. Garner, M.B. Toloczko, S.A Maloy, W.F. Sommer, M.R. James, M. P.D Ferguson, R. Louthan Jr., Shear punch and tensile measurements of mechanical property changes induced in various austenitic alloys by high energy mixed proton and neutron irradiation at low temperatures, J. Nucl. Mater (2000) 418, 283-287.
[34] M.R. James, S.A. Maloy, F.D. Gac, W.F. Sommer, J. Chen, H. Ullmaier, The mechanical properties of an alloy 718 window after irradiation in a spallation environment, J. Nucl. Mater 296 (2001) 139.